



HAL
open science

Towards better understanding of the strain–stress curve of cork : a structure–mechanical properties approach

Massimiliano Gerometta, Xavier Gabrion, Aurélie Lagorce, Sébastien Thibaud, Thomas Karbowskiak

► To cite this version:

Massimiliano Gerometta, Xavier Gabrion, Aurélie Lagorce, Sébastien Thibaud, Thomas Karbowskiak. Towards better understanding of the strain–stress curve of cork : a structure–mechanical properties approach. *Materials & Design*, 2023, 235, pp.112376 (17). 10.1016/j.matdes.2023.112376 . hal-04273685

HAL Id: hal-04273685

<https://hal.science/hal-04273685v1>

Submitted on 7 Nov 2023

HAL is a multi-disciplinary open access archive for the deposit and dissemination of scientific research documents, whether they are published or not. The documents may come from teaching and research institutions in France or abroad, or from public or private research centers.

L'archive ouverte pluridisciplinaire **HAL**, est destinée au dépôt et à la diffusion de documents scientifiques de niveau recherche, publiés ou non, émanant des établissements d'enseignement et de recherche français ou étrangers, des laboratoires publics ou privés.



Distributed under a Creative Commons Attribution - NonCommercial - NoDerivatives 4.0 International License



HAL
open science

Towards better understanding of the strain–stress curve of cork : a structure–mechanical properties approach

Massimiliano Gerometta, Xavier Gabrion, Aurélie Lagorce, Sébastien Thibaud, Thomas Karbowiak

► To cite this version:

Massimiliano Gerometta, Xavier Gabrion, Aurélie Lagorce, Sébastien Thibaud, Thomas Karbowiak. Towards better understanding of the strain–stress curve of cork : a structure–mechanical properties approach. *Materials and Design*, 2023, 235, pp.112376 (17). hal-04273685

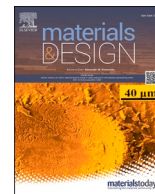
HAL Id: hal-04273685

<https://hal.science/hal-04273685>

Submitted on 7 Nov 2023

HAL is a multi-disciplinary open access archive for the deposit and dissemination of scientific research documents, whether they are published or not. The documents may come from teaching and research institutions in France or abroad, or from public or private research centers.

L'archive ouverte pluridisciplinaire **HAL**, est destinée au dépôt et à la diffusion de documents scientifiques de niveau recherche, publiés ou non, émanant des établissements d'enseignement et de recherche français ou étrangers, des laboratoires publics ou privés.



Towards better understanding of the strain–stress curve of cork: A structure–mechanical properties approach

Massimiliano Gerometta^{a,b}, Xavier Gabrion^b, Aurélie Lagorce^a, Sébastien Thibaud^b, Thomas Karbowiak^{a,*}

^a Univ. Bourgogne Franche-Comté, Institut Agro, PAM UMR A 02.102, 1 Esplanade Erasme, 21000 Dijon, France

^b SUPMICROTECH, CNRS, Institut FEMTO-ST, F-25000 Besançon, France

ARTICLE INFO

Keywords:

Cork structure
Quasi-static compression test
Progressive repeated loading test
Extensometer
Full field measurement
Composite material

ABSTRACT

If the compressive strain–stress curve of cork has already been largely described, its relationship with the cork structure still requires a better understanding. In this study, quasi-static and Progressive Repeated Loading (PRL) tests in compression have been performed on natural cork with a tensile machine. The elastic modulus was measured by a quasi-static compression test on cube or parallelepiped specimens considering different strain measurements methods: crosshead displacement, extensometer, and full field measurements method (Digital Image Correlation or DIC method). Regardless of the considered strain measurement method, the elastic modulus of cork remains in the same order of magnitude. The PRL test carried out at different nominal strains (3 %, 20 %, 46 %, 66 %, 80 %) highlighted the time dependant behaviour of cork (viscous properties). Moreover, a stiffening of the material was observed when increasing the strain at each loading/unloading cycle. Finally, the full field measurement following compression revealed the heterogeneity of the strain distribution on the cork external surface, resulting in localised regions of deformation. From the perspective of compression behaviour, these results lead to a new interpretation of cork which can be considered as a composite material.

1. Introduction

Cork is obtained from the outer bark of the oak tree (*Quercus suber* L.). This lightweight natural material has good chemical stability [1], low permeability to liquids [2], rather high barrier to gases [3] and thermal-acoustic insulation properties [4]. Moreover, it exhibits outstanding mechanical properties, particularly in compression. It is able to undergo large deformations up to 80 % of strain [5]. Cork also displays a fast and important dimensional recovery when the stress is released [6]. All these properties have led to use cork for various applications such as oenology (stoppers), material engineering (expanded cork agglomerates for thermal insulation [7], concrete structure [8], anti-vibration layers [9], ablative insulator in spacecraft [10]), and medicine (therapeutic shoes) [11]. World cork production is about 200 thousand tons per year, with 147 thousand tons (73.5 %) intended for the manufacturing of cork-based stoppers [12].

Cork is an alveolar material that is annually produced by the phellogen activity of the oak tree between April and November. It grows along the radial direction of the tree [13] (Fig. 1a). The outer bark protects the tree from dehydration and fire [14]. Cork is composed of phellem. This botanical term refers to the closed, dead and empty cells.

According to the nomenclature of plant anatomy, the spatial orientation is based on tree growth. The apical growth of the tree corresponds to the axial direction (*z-axis*). Perpendicularly, the stem thickening of the tree represents the radial direction (*y-axis*). The tangential direction (*x-axis*) is orthogonal to both radial and axial directions [13] (Fig. 1a, 1b). As shown by Scanning Electron Microscopy (SEM), cork is an anisotropic material [16] (Fig. 1c). According to the direction of observation, cork cells display a different and characteristic geometrical pattern. In the tangential plane (*x-z axis*), hexagonal cells are connected base to base and organised in staggered rows, arranged in a two-dimensional honeycomb structure. In the transverse plane (*x-y axis*)

* Corresponding author.

E-mail address: thomas.karbowiak@institut-agro.fr (T. Karbowiak).

and radial plane (z - y axis), brick-shaped cells are arranged in parallels rows. Moreover, in the radial plane, the cell walls showed corrugations (Fig. 1c). The thickness of the cell wall is about $1\ \mu\text{m}$ [16].

Phellem is sprinkled with macroscopic channels named lenticels which cross it radially. In the oak tree, their role is to enable gas exchange with the outside environment. As a natural product, cork is a heterogeneous material with a high variability that affects the number and size of lenticels. Lenticels are composed of lignified cells originated from lenticular phellogen with a cell wall 10 times thicker than that of the phellem cells [17]. In the radial or transverse plane, they appear as elongated rectangular channels in the range of $100\ \mu\text{m}$ to a few millimetres thickness, while in the tangential plane, they show a circular/elliptical shape. Lenticels are usually referred to as the porosity of the cork. This parameter is also related to the visual selection used to determine the quality of cork stoppers [13].

In the case of cork stoppers used for bottling wine, the most studied mechanical property is the compressive behaviour of the material [18,19]. For still wines, the stopper (natural or agglomerated cork) is firstly compressed in the bottling machine in the radial and tangential directions. Secondly, it bounces-back to the inner diameter of the bottleneck, that corresponds to a 40 % v/v compression of the material in the bottleneck. In the case of sparkling wines, the compression of the stopper in the bottleneck even reaches 70 % v/v [20]. However, in this case, agglomerated cork is used. The compressive behaviour of agglomerated cork was also studied for construction applications as energy-absorbing material [9], for mobility applications such as helmets used in micro-mobility [21], for motorcycle helmets [22], and in the case of damping and shock absorption, to improve its impact strength [23,24].

The compressive behaviour of natural cork has been extensively studied in the literature. From quasi-static compression test, cork exhibits a mechanical behaviour characteristic of a cellular material. It consists of three regions described as firstly the elastic-like region, then the plateau region and finally the densification region. The stiffness of cork is usually characterized by the elastic modulus calculated from the slope of the elastic region of the nominal strain–stress curve [6,16,25–28]. It has already been shown that several factors can affect the mechanical behaviour of cork such as hydration state [5,19], temperature [25], anisotropy [16,27,28], growth rate [27], cork origin [28], density and porosity [29,30]. With regard to these last two parameters, the corresponding studies revealed that density has a significant influence on the strain–stress curve of cork, with an increase in the resistance to compression for densest cork, considering a selection of different commercial quality classes (good quality – “class 1” and poor quality – “class 4”). However, no clear correlation with porosity was observed. From a general point of view, it is worthy to note that the use of quasi-static compression tests to determine the mechanical properties of cork is tantamount to considering cork as a mechanically homogeneous material. However, this assumption is not really consistent with the physical structure of cork, composed of phellem and lenticels, which have different chemical compositions [17]. This is an important issue in order to better understand the relationship between the structure and the mechanical behaviour of cork in compression. Moreover, the interpretation of the elastic modulus and, in particular, the respective contribution of lenticels and phellem to the stiffness of the material requires further investigation. To that purpose, quasi-static compression tests were performed using not only crosshead displacement and

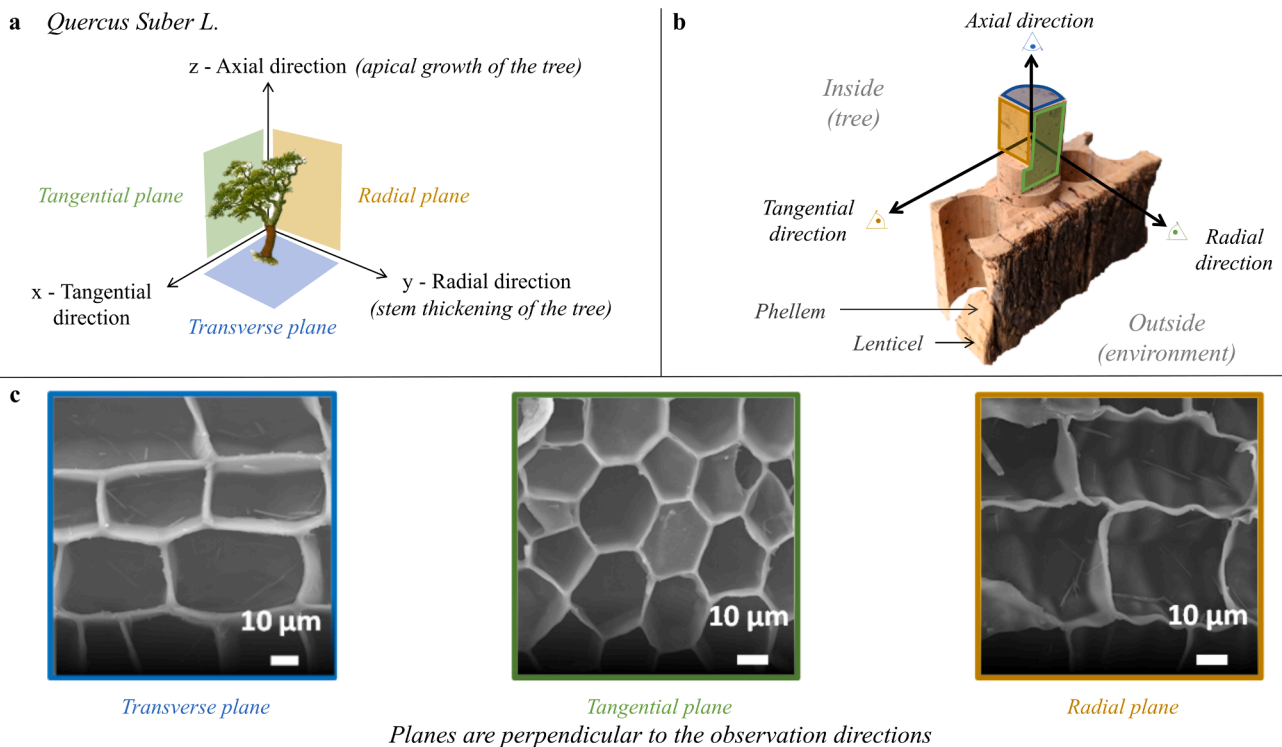


Fig. 1. (a) Spatial reference used to indicate the planes and direction in the cork structure as defined in plant anatomy. (b) Cork macroscopic structure illustrated by a punched bark with a stopper. (c) Scanning Electron Microscopy (SEM) observation from axial direction (or transverse plane in blue), radial direction (or tangential plane in green) and tangential direction (or radial plane in yellow) adapted from [15]. (For interpretation of the references to colour in this figure legend, the reader is referred to the web version of this article.)

extensometer, but also a camera for full field measurement in order to determine the strain fields on the cork surface using the Digital Image Correlation (DIC) method. Although the DIC method has never been used to study the behaviour of natural cork, it has recently been applied to agglomerated cork used in material engineering applications to analyse the strain distribution in heterogenous systems under static [31,32] and dynamic [32] loading. In addition, to study the evolution of the mechanical properties in compression, such as softening/hardening and time dependent behaviour, cork was subjected to a non-monotonic loading by a Progressive Repeated Loading test (PRL).

2. Materials and methods

2.1. Sample preparation

Natural cork stoppers were supplied by the company Bouchon Trescases S.A. (Le Boulou, France). Analyses were performed on cylindrical cork stoppers (24 mm diameter, 49 mm height) referred to as high quality (class 0) without surface treatment. From 14 different stoppers, 14 cubes of $15 \times 15 \times 15 \text{ mm}^3$ and 7 parallelepipeds of $15 \times 15 \times 33 \text{ mm}^3$ were manufactured with a micromilling machine (Kern micro GMBH, Germany). Then, they were stored under controlled conditions of temperature and relative humidity, at $25 \text{ }^\circ\text{C}$ and 53 % RH respectively. To set that RH, magnesium nitrate hexahydrate saline saturated solution was used ($\text{Mg}(\text{NO}_3)_2 \cdot 6\text{H}_2\text{O}$, Sigma-Aldrich, CAS 13446-18-9, Germany). Cork samples were stored until equilibrium was achieved (more than 3 months).

2.2. Mechanical testing

Mechanical testing of cork was performed using an MTS Criterion 45 tensile machine equipped with a 5 kN load cell. Compression tests are performed on each sample along the tangential direction between two parallel steel platens at a crosshead displacement rate of $1 \text{ mm} \cdot \text{min}^{-1}$. The steel platens were covered with polytetrafluoroethylene (PTFE) film (0.125 mm thickness) to reduce the friction coefficient between platens and cork. Strain measurements were realized with three different devices: (i) the displacement of the machine crosshead, (ii) an extensometer (INSTRON 2620) with a gauge length of 12.5 mm and a strain range of $\pm 40 \%$ ($\pm 5 \text{ mm}$) and (iii) a camera to evaluate the strain fields using the Digital Image Correlation (DIC) method, as shown in Fig. 2. Cube

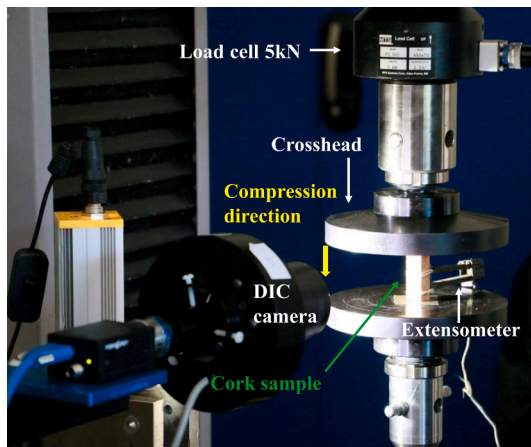


Fig. 2. Quasi-static compression test carried out with crosshead displacement, extensometer and Digital Image Correlation (DIC) camera for the compression of $15 \times 15 \times 15 \text{ mm}^3$ cork cube and $15 \times 15 \times 33 \text{ mm}^3$ cork parallelepiped. Progressive repeated loading test carried out with crosshead displacement for the compression of $15 \times 15 \times 15 \text{ mm}^3$ cork cube.

and parallelepiped geometries (composed of phellem and lenticels) were chosen to compare the different approaches. In particular, the extensometer was used to perform the quasi-static compression test only on parallelepipeds. It cannot be used on cubes due to their too small size and the high strain applied.

2.2.1. Quasi-static compression test

Quasi-static compression tests were carried out on different sample geometries: cubes and parallelepipeds. Raw data were collected directly from the machine acquisition setup. 15 mm edge cubes were compressed along the tangential direction up to 80 % of nominal strain to obtain the full strain–stress curve of the material. For these large strain ranges, this latest was measured by the relative displacement of the machine crosshead. The elastic modulus was calculated in the interval between 1.5 % and 2.3 % of strain, from the slope of the elastic region in which all samples showed a quasi-linear behaviour. When a small deformation is applied ($< 3 \%$ of strain) nominal stress σ_n (MPa) is calculated as the measured force F (N) divided by the initial section area of the sample A_0 (mm^2):

$$\sigma_n = \frac{F}{A_0} \quad (1)$$

The nominal strain ε_n (-) is calculated as follow:

$$\varepsilon_n = \frac{\Delta L}{L_0} \quad (2)$$

With ΔL the relative displacement of the crosshead and L_0 (mm) the initial length.

For higher strain the true or logarithmic stress is calculated and defined by the following relation:

$$\sigma = \sigma_n \times (1 + \varepsilon_n) \quad (3)$$

The associated true or logarithmic strain ε (-) is given by Eq. (4).

$$\varepsilon = \ln(1 + \varepsilon_n) \quad (4)$$

Quasi-static compression test was also carried out on $15 \times 15 \text{ mm}^2$ base and 33 mm height rectangular parallelepipeds, which were vertically compressed along the tangential direction up to 10 % of strain. For this geometry, above this strain the sample exhibits buckling phenomena as shown in Fig. 3.

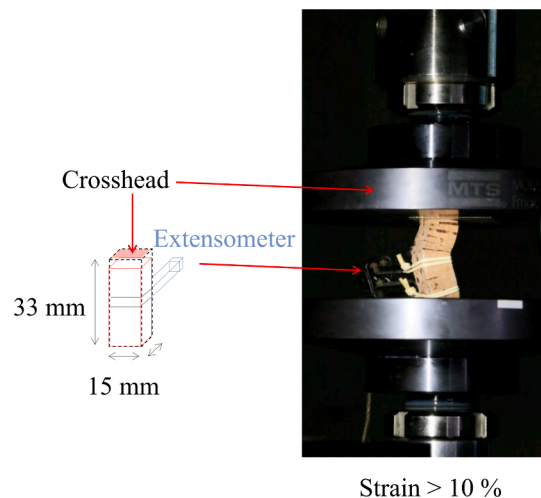


Fig. 3. Buckling phenomenon observed for parallelepiped of $15 \times 15 \text{ mm}^2$ base and 33 mm height during the quasi-static compression test carried out with the crosshead displacement and the extensometer.

The strain was measured from the relative displacement of the machine crosshead and the extensometer. For comparison purposes, a specific strain range for each analysis was selected in the elastic region, in which all samples showed a quasi-linear behaviour. Two ranges were considered: from 0.4 % to 1.2 % of strain (crosshead case) and from 0.4 % to 0.8 % of strain (extensometer case).

2.2.2. Digital image Correlation (DIC)

In the case of the quasi-static compression test, Digital Image Correlation (DIC) method was simultaneously used. DIC is a non-contact optical technique used to determine the full field measurements of a sample surface by measuring the displacement of pixels in digital images after deformation compared to a reference image [33]. The images were recorded with VIC®-Snap software using a PointGrey® GrassHopper camera equipped with a telecentric objective Edmund 0.20x (Fig. 2). This lens enables constant magnification regardless of the object's distance or location in the field of view. Therefore, the measurements of the dimensions of an object will be independent of its position. For cubes, 60 images were acquired in the first minute and then 20 images per minute until the end of the test. For parallelepipeds, 60 images per minute were acquired during the test. Post-processing images for the calculation of the strain field, for both geometries, were carried out by using Ufreckles V 2.0 software [34]. The image registration is based on the optical flow equation as defined below:

$$f(x) = g(x + u(x)) \tag{5}$$

where f is the reference image, g the deformed picture and u the searched displacement field. Using the Ufreckles software, Eq. (5) is solved by using a non-linear least-squares algorithm as given in Eq. (6).

$$Er^2 = \sum [f(x) - g(x + u(x))]^2 \tag{6}$$

The algorithm normalizes the grey level of the image minimizing the influence of lighting variation. A mesh is generated to interpolate the displacement field with four nodes quad elements [34]. The region of interest (ROI), manually selected on the cork surface, is associated to a rectangular area used to interpolate the displacement field. This zone does not include the boundary zone of the sample to prevent edge imperfections from corrupting the results. The DIC camera is connected to the tensile machine to record the load. The stress (MPa) as a function of strain (y axis; compression direction) is plotted. Following the data treatment with Ufreckles software, the elastic modulus is calculated

from the slope of the elastic region in which samples showed a quasi-linear behaviour.

The Poisson's ratio has been calculated based on the DIC method during the quasi-static compression test. The pixel displacement for two directions (x, y axis) is extracted from the comparison of pattern displacement between two consecutive images. The x axis corresponds to the transverse axis (perpendicular to the compression direction), while the y axis represents the longitudinal direction in which cork sample is compressed by the crosshead as defined in Eq. (7).

$$\nu = -\frac{\epsilon_{xx}}{\epsilon_{yy}} \tag{7}$$

Following the data treatment with Ufreckles software, the transverse strain (ϵ_{xx}) as a function of the longitudinal strain (ϵ_{yy}) is plotted. With DIC method, mean values of transverse and longitudinal strain fields are computed. Finally, a linear regression was used to obtain the Poisson's ratio mean values for each sample. The same procedure is used for the calculation of the elastic modulus. For both geometries, the elastic modulus and the Poisson's ratio for non-radial directions were calculated in the elastic region in the interval set between 0.1 % and 1.5 % of strain. Poisson's ration is extracted, in relation with Fig. 5, from zone 1 (Elastic-like behaviour).

In addition, for cubes, the image thresholding analysis was performed on the strain fields measured at 1 %, 5 %, 10 % and 15 % of strain. From this analysis, the percentage of lenticels on the surface of the cork cube and the corresponding percentage of compression was calculated. Tests were performed on 7 replicates for both geometries.

2.2.3. Progressive repeated loading test (PRL)

Five successive loading-unloading cycles were applied on cubes, with a crosshead displacement rate of $1 \text{ mm}\cdot\text{min}^{-1}$, at increasing nominal strains of 3 %, 20 %, 46 %, 66 % and 80 %, corresponding to the different regions (elastic, plateau and densification) of the characteristic nominal strain-stress curve. Following the procedure summarised in Fig. 4, cork cube was first loaded by the crosshead displacement up to a defined strain, then unloaded until the crosshead returned to its initial position (no strain applied to the sample for each cycle), before starting a new cycle immediately.

The evolution of tangent modulus at different strain values allows to determine the evolution of the material stiffness under progressive repeated loading. In case of monotonic tests (tensile or compression tests), it is not possible to evaluate this evolution. The test was

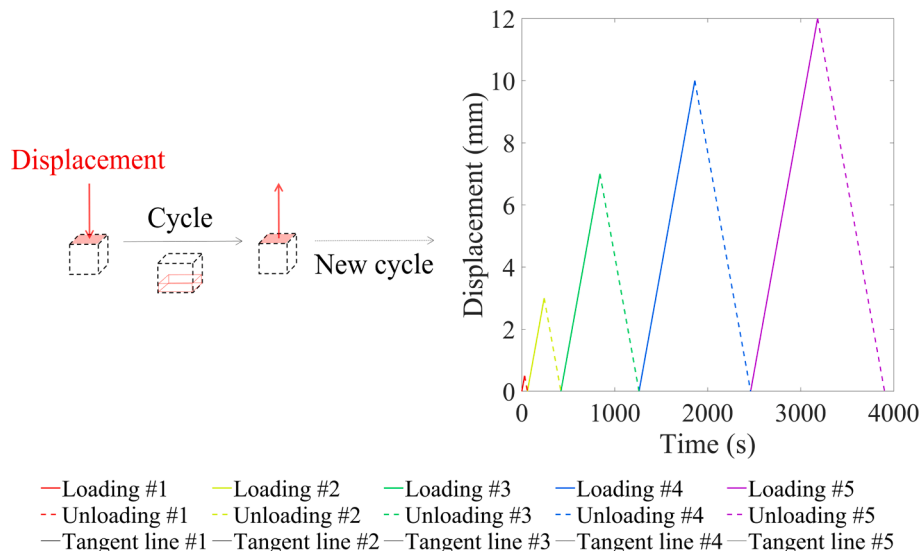


Fig. 4. Crosshead displacement at increasing strains values as a function of time for PRL test corresponding to the five loading/unloading cycles.

performed on 4 different samples. The tangent modulus was calculated from the true and nominal strain–stress curves of the unloading cycles. A third order polynomial was interpolated over the first 200 points, then, a derivation of the third order polynomial function was applied.

2.3. Statistical analysis

Statistical analyses were performed on data obtained from quasi-static and progressive repeated loading (PRL) tests in compression. The Student's *t*-test (*p* value < 0.05) was used to compare the mean value of the elastic modulus measured by the crosshead displacement and DIC for cubes. For parallelepipeds, one-way ANOVA with a Tukey's multiple comparison test was used (*p* value < 0.05) to compare the mean value of the elastic moduli obtained for each strain measurement method: crosshead displacement, extensometer and DIC. For the PRL test, one-way ANOVA was used to compare the tangent modulus obtained for each of the five unloading cycles. The Student's *t*-test (*p* value < 0.05) was used to compare the respective values of the nominal and true tangent moduli for each unloading cycle.

3. Results and discussion

3.1. Determination of the initial elastic modulus of cork from monotonic compression test

The mean strain–stress curve of the cork cubes obtained from quasi-static compression tests is shown in Fig. 5. The 95 % distribution corresponding to all values of strain–stress curves of cork cubes (*n* = 6) is also represented by the red area in Fig. 5. Cork samples were compressed up to 80 % of nominal strain in the tangential direction, as detailed in the materials and methods section. The typical mechanical behaviour of cork material is shown in Fig. 5. As already reported in many studies [16,27–29] three distinct regions can be distinguished. In the first region, up to 3 % of strain, cork shows an elastic-like behaviour (Fig. 5, zone 1). A stress value close to 0.5 MPa is reached. Then, between 3 % and 55 % of strain, a horizontal plateau is observed (Fig. 5, zone 2). It corresponds to the progressive buckling of the cell walls. In this region, cork presents a constant stress value of approximately 1 MPa. Finally, above 55 % of strain, a densification region is characterised by the collapse of the cells (Fig. 5, zone 3). This gives a sharp increase in the stress values, from 1 MPa to 8 MPa.

The elastic modulus (*E*, MPa) of cork was calculated in the elastic region from the slope of the nominal strain–stress curve (Fig. 5, zone 1). An average value of 19.7 ± 5.1 MPa was calculated for the quasi-static

compression test carried out with the crosshead displacement. As reported in Table 1, the compressive behaviour of cork under environmental conditions similar to the present study (temperature and relative humidity) have been thoroughly investigated in the literature. From tangential compression, Anjos *et al.* found similar values on 20 mm edge cork cubes, with elastic modulus values between 11.2 ± 1.7 MPa and 19.1 ± 4.5 MPa [29,30]. Similarly, Fortes and Nogueira carried out compression testing on 30 mm edge cork cubes in the non-radial direction, reporting a value of 19 MPa [26]. All these previous studies converge towards the fact that cork exhibits a higher stiffness in the radial direction with an average elastic modulus of 16.8 MPa, which is approximately 27 % higher than those obtained in the non-radial directions with a mean value of 12.3 MPa (axial and tangential) [5,6,16,25–30]. However, it is worthy to note the very high variability of the elastic moduli, as reported in Table 1, with values ranging from 5.9 MPa to 46.9 MPa for the radial direction and from 3.1 MPa to 22.1 MPa for the non-radial direction. This wide range of values can be explained by the biological origin of cork and the environmental conditions to which it is exposed, which can affect the annual growth ring and thus the density of cork. In addition, the high variability of the porosity, from good quality class (class 0) to poor quality class (class 4), can also have an impact on the mechanical properties. Regarding the way of performing test, it is also interesting to note that the quasi-static compression tests performed with the crosshead displacement were not performed in standardised conditions in term of (i) solicitation rate, (ii) sample size, (iii) temperature and relative humidity. To date, there is indeed no international standard method for studying the mechanical behaviour of cork material in compression. The only exception is for cork stoppers, for which a simplistic standard exists for determining the dimensional recovery under compression after three minutes, following the bottling operation [35].

In the field of material engineering, extensometer is commonly used as a standard device to measure the strain for materials such as metals, composites, or polymers. For this reason, it was selected in this study to determine the elastic modulus of cork. In this case, cork parallelepipeds were vertically compressed along the tangential direction up to 10 % of nominal strain. The strain–stress curve, up to 6 % of strain, obtained using the crosshead and the extensometer, are shown in Fig. 6. The tangent line represents the selected strain interval in the elastic region of each curve where the elastic modulus (*E*, MPa) was calculated.

Digital Image Correlation (DIC) method was also used to determine the elastic modulus of cork. In addition, this method also measured the strain in the transverse direction, perpendicular to the compression direction. In this case, the Poisson's ratio for non-radial directions was calculated as the ratio between transversal and longitudinal strain. For comparison purpose, Table 2 shows the values of the elastic moduli obtained from quasi-static compression tests, as provided by crosshead displacement, extensometer and DIC methods. The value of Poisson's ratio is also shown for both sample geometries.

For parallelepipeds geometry, an average value of 23.0 ± 1.1 MPa, 30.1 ± 3.7 MPa and 24.9 ± 1.6 MPa was measured with the crosshead, the extensometer, and DIC, respectively. The value determined from extensometer is significantly different from the those obtained from crosshead and DIC methods. The latter two did not show significant difference. On the contrary, in the case of cork cubes, these two methods gave significantly different values, with 19.7 ± 5.1 MPa and 30.8 ± 4.2 MPa, respectively. Moreover, regardless of the method used to determine the elastic modulus of cork, the variability of the data remain in the same order of magnitude. The Poisson's ratio, with an average value of 0.34 ± 0.07 for cork cubes and 0.33 ± 0.03 for cork parallelepipeds, was determined for the non-radial directions. They are in the same order of magnitude as the values from Gibson *et al.* and Fortes and Nogueira, who reported a Poisson's ratio for non-radial directions of 0.5 ± 0.05 and 0.26 (standard deviation not given for this last value), respectively. The small discrepancy that appears between these results can be attributed to the dimensions of the sample and the device used to measure the Poisson's ratio (a DIC camera was used in this study while an extensometer was used in the two other studies). These values are three times higher than those

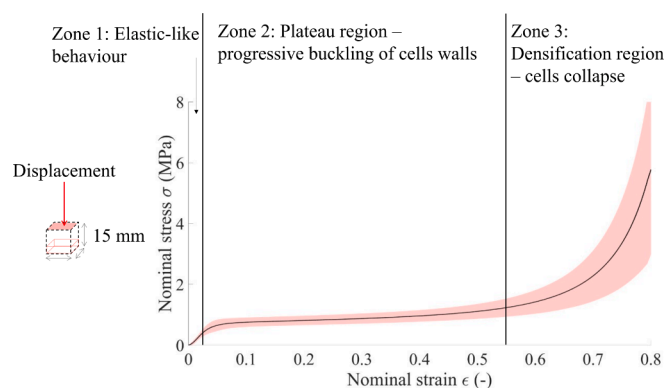


Fig. 5. The mean strain–stress curve (black line) obtained from quasi-static compression tests performed with a constant crosshead displacement rate of $1 \text{ mm}\cdot\text{min}^{-1}$ on $15 \times 15 \times 15 \text{ mm}^3$ cork cubes compressed up to 80 % of nominal strain (*n* = 6). All samples were compressed parallel to the tangential direction. (Red area: confidence interval at 95 %). (For interpretation of the references to colour in this figure legend, the reader is referred to the web version of this article.)

Table 1

Values of elastic modulus of cork found in the literature for the radial, axial and tangential directions, obtained from a quasi-static compression test. Values are expressed as average \pm standard deviation. (N/A = not available, N/D = not determined).

Cork sample	Quasi-static compression test conditions						Elastic modulus, E (MPa)			Ref.
	Geometry (h \times l \times w) (mm ³)	Test speed (mm·min ⁻¹)	T (°C)	RH (%)	Strain interval (%)	Direction				
						Radial	Axial	Tangential		
Commercial cork	15 \times 15 \times 15	N/A	N/A	N/A	N/A	20 \pm 7	13 \pm 5	13 \pm 5	[16]	
Low porosity cork	20 \times 20 \times 20	2	N/A	N/A	1 - 1.5	16.8 \pm 5.8	14.8 \pm 0.9	12.4 \pm 2.3	[25]	
		0.2				6.0 \pm 2.2	3.1 \pm 0.8	4.9 \pm 0.8		
Low porosity	16 \times 16 \times 16	2	20	N/A	1 - 1.5	7.1 \pm 1.5	4.0 \pm 2.3	8.5 \pm 1.5	[6]	
		20				13.0 \pm 1.2	6.0 \pm 0.3	12.5 \pm 1.0		
Low porosity cork	30 \times 30 \times 30	3.8	N/A	N/A	1 - 2	29		19	[26]	
Large cork	20 \times 20 \times 20	2	N/A	N/A	1 - 1.5	9.9 \pm 0.4	9.2 \pm 0.5	7.9 \pm 1.3	[27]	
Medium cork	13.2 \pm 0.7					12.0 \pm 1.5	9.6 \pm 1.4			
Small cork	11.5 \pm 1.0					10.9 \pm 0.6	8.6 \pm 0.7			
Low porosity cork	N/A	$1.6 \times 10^{-3} \text{ s}^{-1}$	N/A	6	0 - 5	10.0		7.0	[36]	
						5.9		5.2		
Raw cork planks (class 1)	20 \times 20 \times 20	2	N/A	N/A	1 - 2.5	17.9 \pm 2.9	16.6 \pm 1.8	13.4 \pm 1.4	[29]	
Raw cork planks (class 4)						18.6 \pm 3.3	17.1 \pm 2.3	11.2 \pm 1.7		
Low density 130–150 kg·m ⁻³	20 \times 20 \times 20	2	N/A	N/A	1 - 2.5	17.4 \pm 4.5	16.6 \pm 3.3	14.4 \pm 4.8	[30]	
Mid density 150–190 kg·m ⁻³						22.6 \pm 5.1	16.3 \pm 2.6	16.8 \pm 3.9		
High density 190–250 kg·m ⁻³						26.1 \pm 4.5	18.5 \pm 5.2	19.1 \pm 4.5		
Planks from oak forest	18 \times 18 \times 18	2	N/A	N/A	1 - 2	10.4 \pm 3		9.2 \pm 2.6	[28]	
Natural raw cork stoppers (class 0)	15 \times 15 \times 15	60	25	53	N/A	46.9 \pm 8.1	N/A	22.1 \pm 2.0	[5]	
Natural cork stoppers (class 0)	15 \times 15 \times 15	1	25	53	1.5 - 2.3	N/D	N/D	19.7 \pm 5.1	Present work	

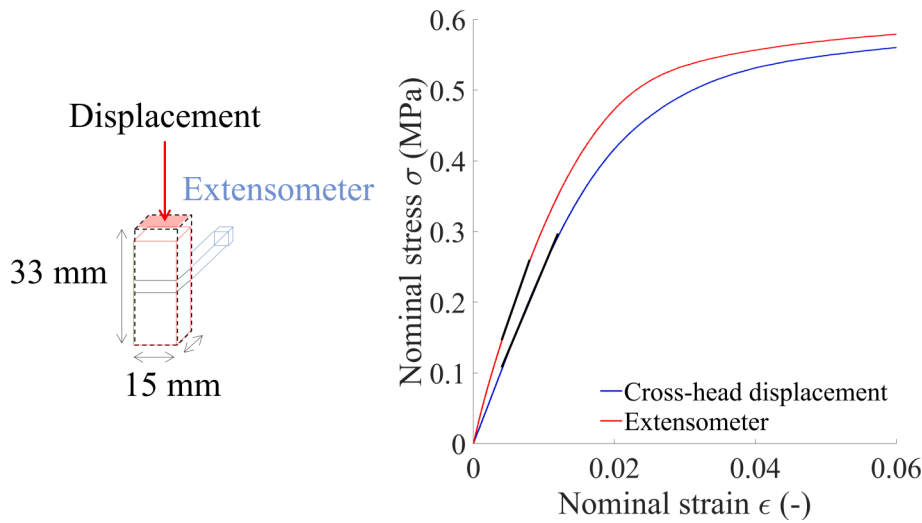


Fig. 6. Strain-stress curve obtained from quasi-static compression test: comparison between crosshead and extensometer. Measurements were carried out on parallelepipeds of $15 \times 15 \text{ mm}^2$ base and 33 mm height compressed up to 6 % of nominal strain parallel to the tangential direction ($n = 7$). Black tangent lines represent the range selected for the elastic modulus calculation: from 0.4 % to 1.2 % of strain (crosshead) and from 0.4 % to 0.8 % strain (extensometer).

reported for the radial/non-radial and non-radial/radial directions, with a value of 0.097 and 0.064 [16,26]. The results obtained from the quasi-static compression test showed that the determination of the elastic modulus of cork is affected by the method used for the strain measurements. Crosshead displacement corresponds to a global measurement of the rigid displacement between the fix and mobile steel platens. When using this method, cork is therefore considered as a homogeneous material in which a uniform stress distribution is applied. This is obviously a simplifying assumption, given the morphology of cork. Similar to the strain measurement performed with the crosshead displacement, when using the extensometer, cork is also assumed to be a homogeneous material. This method is based on a local measurement of the strain in the middle of the sample. The presence of the extensometer positioned on a selected region of the sample can induce a local increase of the material stiffness due to the pressure applied by the elastic bands attached to the surface of the sample. This leads to a higher value of the elastic modulus. On the contrary, DIC clearly revealed a heterogeneous strain distribution on the cork surface, providing spatial information about the macroscopic deformation of cork (Fig. 8). The respective contribution of lenticels and phellem to the stiffness of the material will thus be further discussed in more details. Finally, it's worth pointing out that the extensometer and DIC methods can only be used to study the first part of the strain-stress curve, up to 10 % and 15 % of strain, respectively. On the contrary, the strain measured with the crosshead displacement provide the full strain-stress curve, up to 80 % of strain. To further investigate the strain-stress curve and to better understand its relationship with the cork structure, a progressive repeated loading test was also performed in this

study.

3.2. Response of the cork material to Progressive Repeated Loading (PRL) cycles

In addition to the investigation of the behaviour of cork under monotonic compression test, the response of the material to successive compression cycles was also studied. Fig. 7a shows the regions of the nominal strain-stress curve and the corresponding nominal strain values for which PRL test was performed. A typical nominal and true strain-stress curve obtained for five successive cycles are displayed in Fig. 7b and 7c, respectively. Each curve consists in a loading and unloading cycle. The loading curve of the 1st and 2nd cycles are characterised by an initial single linear slope, while for the successive loading curve of the 3rd, 4th, and 5th cycles, different slopes are observed (Fig. 7b and 7c). As displayed in Fig. 7d, a tiny hysteresis between the loading and unloading curve is noticeable for the 1st cycle. Moreover, when cork is compressed up to 20 % of strain, the 1st and 2nd loading cycles overlap (Fig. 7d). On the contrary, from the 2nd to the 5th cycle the hysteresis between the loading and unloading curve becomes more important. In addition, between the 2nd and 3rd, 3rd and 4th and 4th and 5th cycle the loading curves do not overlap and a stress loss appears (Fig. 7e). This indicate that a part of cork does not recover its original shape between two successive cycles. It is noteworthy that after each of the five successive compressive cycles, cork does not exhibit the same mechanical behaviour. By definition, the elastic modulus is calculated from the slope of the elastic region of the true strain-stress curve. In the case of cork, it is

Table 2

Elastic modulus values obtained from the slope of the elastic region of the nominal strain-stress curves when a quasi-static compression test is applied on cork cubes ($n = 6$) and parallelepipeds ($n = 7$) using the crosshead displacement, extensometer and DIC methods. The extensometer cannot be used on cubes because of their too small size and too high strain applied. Poisson's ratio is also reported for non-radial directions measured for cork cubes and parallelepipeds by DIC. Values are expressed as average \pm standard deviation. Statistics: One-way ANOVA (Significant differences, with p value < 0.05 , are indicated with different letters. a, b: difference between strain measurement methods for cork cubes. α , β : difference between strain measurement methods for parallelepipeds). (N/A = not available).

Method	Elastic modulus, E (MPa) from nominal strain-stress curve		
	Cork sample geometry		
	Cube $15 \times 15 \times 15 \text{ mm}^3$	Parallelepiped $15 \times 15 \times 33 \text{ mm}^3$	
Crosshead displacement	19.7 ± 5.1^a		$23.0 \pm 1.1^\alpha$
Extensometer	N/A		$30.1 \pm 3.7^\beta$
Digital Image Correlation (DIC)	30.8 ± 4.2^b		$24.9 \pm 1.6^\alpha$
	0.34 ± 0.07	Poisson's ratio, $\nu_{NR/NR}$	
			0.33 ± 0.03

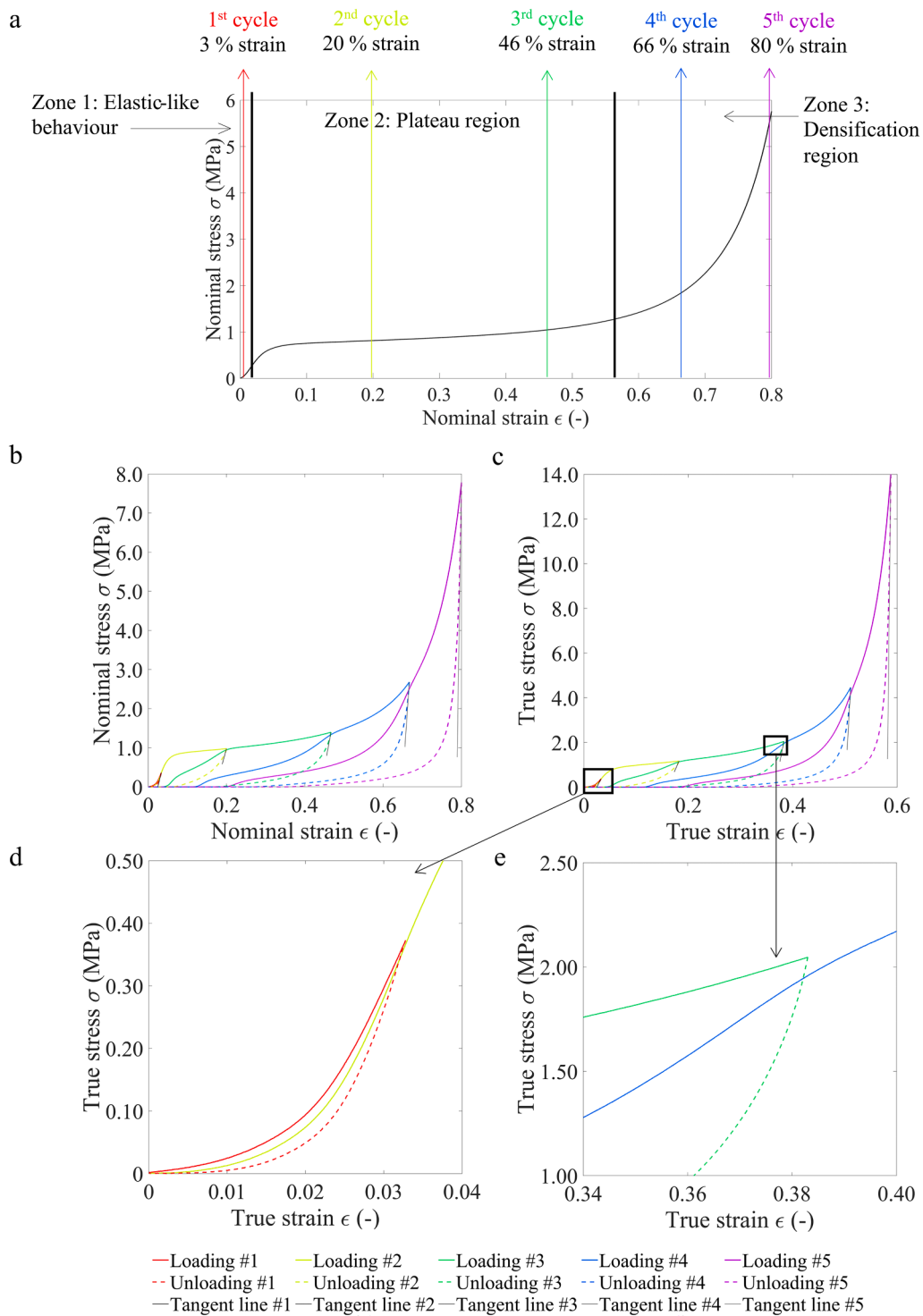


Fig. 7. (a) Representation of the region of the nominal strain–stress curve in which the PRL test was performed. (b) Nominal strain–stress curve obtained for five consecutive progressive cycles performed on cork cube. (c) True strain–stress curve obtained for five consecutive progressive cycles performed on cork cube. (d) Hysteresis phenomenon observed between loading and unloading on the 1st cycle (1st and 2nd loading curves overlap). (e) Stress loss observed between 3rd and 4th loading curves.

calculated from the nominal strain–stress curve, in all studies (as reported in Table 1). When cork is subjected to small deformation (up to 3 % of strain), the nominal elastic modulus is similar to the true elastic modulus. However, when cork is subjected to larger deformation these values are different. In large deformation, the effect of the instantaneous cross-sectional area is not negligible. In such a case, there is no linear correlation between strain and stress fields, thus making the calculation

of the elastic modulus not accurate. Moreover, in the case of the PRL test, it was not possible to calculate the elastic modulus from the slope of the linear region of each loading curve because different slopes were observed for the 3rd, 4th and 5th cycles (Fig. 7b and 7c). For this reason, a tangent modulus was calculated from each unloading cycle, considering the slope of the linear region for both the true and nominal strain–stress curves (tangent line, Fig. 7b and 7c).

Table 3

Tangent modulus (MPa) calculated from the true and nominal strain–stress unloading curves for each unloading cycle in the PRL test. Values are expressed as average \pm standard deviation. Statistics: One-way ANOVA (Significant differences, with p value < 0.05 , are indicated with different letters. a, b: difference between the 5 cycles for the true tangent modulus. γ , δ difference between the 5 cycles for the nominal tangent modulus). T-student test (Significant differences, with p value < 0.05 , are indicated with different letters. α , β : difference between the corresponding cycle for the true tangent and nominal tangent moduli).

Unloading cycle	Tangent modulus (MPa)	
	True strain–stress curve	Nominal strain–stress curve
1	34.9 \pm 13.4 ^{a, α}	32.4 \pm 12.4 ^{γ, α}
2	45.4 \pm 8.4 ^{a, α}	30.8 \pm 5.8 ^{γ, β}
3	94.7 \pm 23.8 ^{a, α}	43.3 \pm 11.0 ^{γ, β}
4	331.6 \pm 101.3 ^{a, α}	118.2 \pm 36.5 ^{γ, β}
5	1806.0 \pm 624.0 ^{b, α}	554.3 \pm 193.4 ^{δ, β}

The tangent moduli values are given in Table 3. For the true tangent modulus, a monotonic evolution was observed from the 1st to the 5th unloading cycle, which values from 34.9 MPa to 1806.0 MPa. Similarly, the nominal tangent modulus values increased from 32.4 MPa to 554.3 MPa. For both cases, only the 1st cycle is significantly different from the 5th cycle, while the 2nd, 3rd and 4th cycles are not different, highlighting the high heterogeneity of cork as a natural material. It is also worthy to note that the 1st unloading cycle of the true and nominal tangent moduli are not different, whereas from the 2nd to the 5th cycles, they shown significance difference. Furthermore, the values of the tangent modulus of the 2nd, 3rd, 4th and 5th cycles calculated from the true strain–stress curve were higher compared to the corresponding value obtained from the nominal strain–stress curve. This result confirms that when cork is subjected to small deformations, the tangent moduli calculated either from the true or from the nominal strain–stress curve are not significantly different.

The stiffening of the material observed when increasing the strain at each loading/unloading cycles may be due to structural changes occurring in cork. The overlapping of the first two cycles reveals that when cork is subjected to small deformations (3 % of strain), it responds as an elastic material and only reversible modifications in the cork structure occur. In contrast, following large deformation (> 20 % of strain), the stress loss observed between successive cycles show that cork exhibits a time dependant behaviour (viscoelastic behaviour). It increases from 2 % for the 2nd–3rd cycles to 7 % for the 4th–5th cycles (Fig. 7e). This indicates delayed modifications in the material structure which can be attributed to the viscous component. Furthermore, the contribution of the viscous component of the material to its mechanical behaviour is also highlighted by the large hysteresis observed between

loading and unloading curves (from the 2nd to the 5th cycles). Unambiguously, cork is a viscoelastic material. Its strain–stress curve is characterised with an elastic region in which the material returns to its original state once the stress is removed, and a viscous region, in which, it does not fully recover [37]. The hysteresis and the stress loss phenomena observed following the PRL test, can be attributed to structural changes of the cell walls. At large deformation, a buckling phenomenon occurs, and the cell wall network starts to deform non-homogeneously. This first hypothesis may explain the change in the slope of the loading curves observed for the 3rd, 4th and 5th cycles. Concerning the stress loss observed between 2nd and 3rd, 3rd and 4th, 4th and 5th loading curves (Fig. 7e), two hypotheses can be formulated. Firstly, it can be assumed that the application of a large deformation, the cell walls undergo irreversible structural damage which does not allow them to fully recover. Secondly, the viscous component of the cell walls may be characterised by multiple relaxation times, ranging from instantaneous to extremely slow recovery. Rosa and Fortes observed an almost full dimension recovery (less than 1% of residual deformation in the compression direction) of 16 mm edge cork cubes subjected to quasi-static compression test at 30 % of strain at 20 °C after 20 days. In contrast, when a larger strain up to 80 % was applied, a permanent deformation was observed even after 70 days (more than 5 % of residual deformation in the compression direction) [6]. In another study, the same authors investigated the stress relaxation and creep behaviour of cork. They used a compression test with loading-relaxation-unloading cycles applied on cork in order to simulate the performance of a cork stopper (30 % of strain compression in the tangential direction, 10 min relaxation, 10 min in unloaded condition, 10 cycles). The loss in dimensional recovery of cork was attributed to stress relaxation phenomenon associated with the unfolding process of the buckled cell walls [38]. In a more recent study about the viscoelastic properties of cork, suberin was assumed to be the macromolecule responsible for this phenomenon [37].

According to its alveolar structure, the mechanical behaviour of cork in compression can also be compared with that of other cellular materials. Polymeric foams, manufactured from polymers such as polyurethane (PU), polystyrene (PS), polyethylene (PE), polypropylene (PP), polyethylene vinyl acetate (EVA), nitrile rubber (NBR), polyvinyl chloride (PVC), and other polyolefins [39], exhibit a compressive mechanical behaviour comparable to that of cork. Their strain–stress curve also shows three distinct regions. In the first region, up to 10 % of nominal strain, the foams show a quasi-linear elastic deformation in which the elastic bending of the cell edges and the elongation of the cell faces occurs. Then, they are characterised by a flat plateau region with an almost constant stress value up to ~ 60 % of strain, in which the cell edges collapse occurs. Finally, above ~ 60 % of strain, the foams exhibit

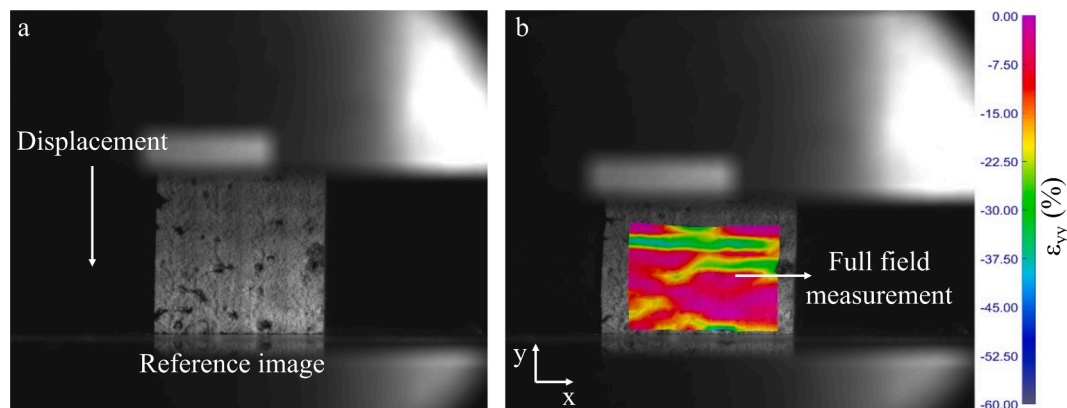


Fig. 8. Digital Image Correlation method: (a) reference image of the natural cork cube used to measure the displacement of pixels along y-direction. (b) Strain measurement ϵ_{yy} (%) displayed as a full field on the cork cube surface represented by a rectangle coloured isovalues. The pink areas show the pixels which moved the less, while the blue regions correspond to the regions where the pixels displacement is the most important. (For interpretation of the references to colour in this figure legend, the reader is referred to the web version of this article.)

a densification region in which the stress increases sharply, characterised by the collapse of the cells [4]. Sun *et al.* studied the mechanical behaviour of polymer foam (polymethacrylimide, PMI) subjected to loading–unloading cycles up to 95 % of strain. They noted that the loading–unloading curves exhibit a viscoelastic hysteresis, mainly resulting from the viscosity of the cell-wall material. This hysteresis was rather limited between unloading and reloading curves for strains lower than 30 %, while for larger strains it became more marked [40]. In another study, Ramsteiner *et al.* analysed the deformation behaviour of polymer foam (polystyrene, PS). They found that the deformation behaviour of this polymer foam in compression is inhomogeneous. The cells are destroyed heterogeneously, with highly densified regions next to undeformed regions [41]. A similar phenomenon is observed for cork in which the deformation behaviour could be attributed to a structural change in the phellem cell walls and/or in the lenticels cell walls. Thus, cork may be considered as a cellular damaged material when large deformation is applied (up to 80 % of nominal strain).

3.3. Contribution of lenticels to the mechanical properties of cork in compression

Digital image correlation (DIC) was used to measure the strain fields on the cork sample subjected to a quasi-static compression test. Fig. 8a shows a reference image of a $15 \times 15 \times 15 \text{ mm}^3$ natural cork cube composed of phellem (cork cells) sprinkled with lenticels. An example of post-processing DIC analysis is shown in Fig. 8b. The strain ϵ_{yy} (%) measured along the crosshead displacement direction (y -axis) is displayed as a full field measurement of the cork surface. It is represented by a rectangle coloured with isovalues according to pixels displacement.

A typical DIC analysis carried out on natural cork compressed at 1 %, 5 %, 10 %, and 15 % of nominal strain is reported in Table 4. The full field measurement of the cork cube surface obtained for each strain is displayed as a rectangle, coloured according to the strain distribution. The pink areas correspond to the regions in which pixels moved the less, while blue regions correspond to the regions where the pixels displacement is the most important. The corresponding images before and after thresholding analysis (application of a binarization filter) are also displayed. From these last images, the lenticels proportion was calculated for each strain applied to the sample, as well as the proportion of shrunk lenticels following the compression. Data obtained for the other samples are provided in the appendix. A first observation of the DIC images reveals that when cork is compressed, the initial cross-sectional area in contact with the crosshead changes. By compressing cork from 1 % to 15 % of strain, the surface in contact with the crosshead becomes larger, while the transverse section is smaller. Moreover, the strain-field images clearly highlight that the deformation is not uniformly distributed throughout the material. Indeed, localised regions of strain appears between phellem and lenticels. Particularly, in the region around lenticels the highest strain level is observed, representing a very localised strain (stress concentration at the lenticel's interface). This observation is also supported by the fact that the percentage of lenticels decreases from 3.4 %, before applying the compression test, to 2.2 % when applying strain at 15 % on cork cube. This clearly reveals a shrinkage of lenticels which is even more important when the nominal strain is applied. On the contrary, in the phellem area without lenticel, the strain is more homogeneously distributed. This phenomenon was observed for all samples analysed. These results clearly evidenced the heterogeneous behaviour of cork when subjected to compression highlighting the fact that cork itself can be considered as a composite material. In the literature, Anjos *et al.* already studied the effect of the lenticular porosity on the compressive behaviour of cork. Good quality (small and few lenticels) and poor-quality cork planks (high number of lenticels with large cross-section area) were compressed up to 80 % of strain at a constant crosshead displacement rate of $2 \text{ mm} \cdot \text{min}^{-1}$. As the strain–stress curves obtained were similar for both quality classes with different porosities, they concluded that the effect of the porosity on the

compression of cork was not significant. Nevertheless, a trend towards an overall increase in stress with porosity was noticeable for strains above 25 % [29]. To date, there is no data available in the literature on the use of DIC for natural cork. If DIC has already been recently applied to study the mechanical properties of agglomerated cork, therefore a composite internal with polyurethane adhesive [31,32], it is the first time that is applied on natural cork. Therefore, these results highlight that the respective role of lenticels and phellem is of fundamental importance to better understand the relationship between the structure of cork and its compression properties.

4. Conclusions

This study investigated the compressive mechanical behaviour of natural cork. To this end, the elastic modulus of cork was determined by a quasi-static compression test using the crosshead displacement, the extensometer and the Digital Image Correlation (DIC) methods. Although different values were obtained according to the different strain measurements methods, they remain in the same order of magnitude. The response of the material to five successive compression cycles was also studied by progressive repeated loading (PRL) test. From the strain–stress curve of the 3rd, 4th and 5th loading cycles, different slopes were observed which highlight changes in cellular structure of cork. The tangent modulus was calculated from each unloading cycle. It increased with the increasing strain of loading/unloading cycles, from the 1st to the 5th, showing a strong stiffening of the material. Furthermore, from the 2nd to the 5th cycles, a huge hysteresis and a stress loss were observed on the corresponding strain–stress curves, revealing the time dependent properties of cork, particularly its viscous component, which are characterised by several relaxation times. Finally, DIC unveiled the heterogeneity of the strain distribution throughout cork under compression, showing localised regions of strain between the phellem and lenticels, which leads to consider cork as a composite material. In particular, the qualitative results obtained by the DIC method applied to the quasi-static compression test represents a first step towards a better understanding of the structure–mechanical property relationship of cork. To go further in understanding the compressive behaviour of cork, the respective role of the phellem and the lenticels should be investigated by non-destructive *in-situ* image analysis at the microscopic scale. Moreover, the relaxation phenomena related to the viscous component in the cork structure should be studied in more details.

Declaration of Competing Interest

The authors declare that they have no known competing financial interests or personal relationships that could have appeared to influence the work reported in this paper.

Data availability

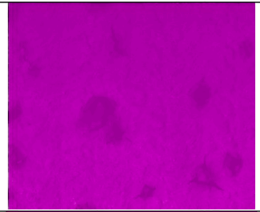
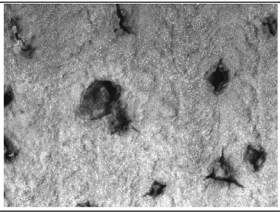
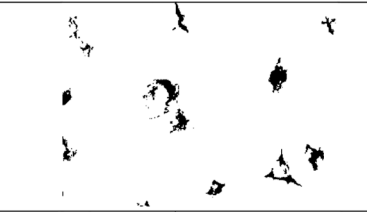

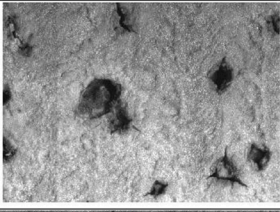
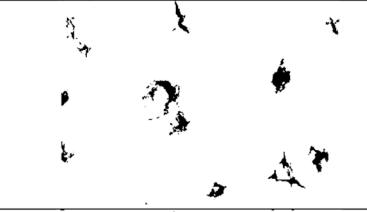
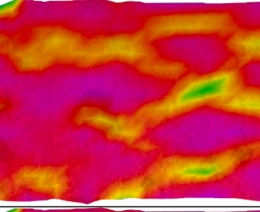
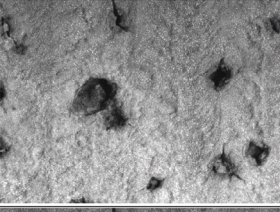
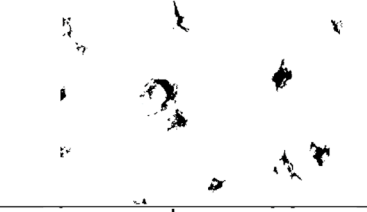
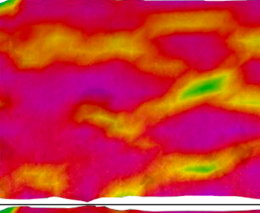
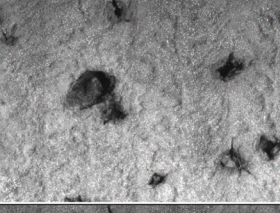
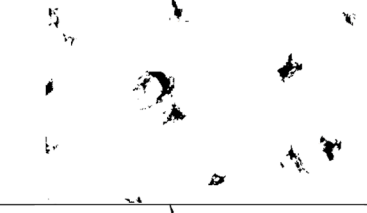
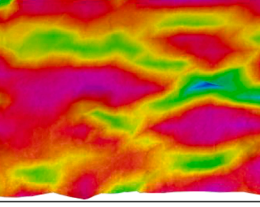
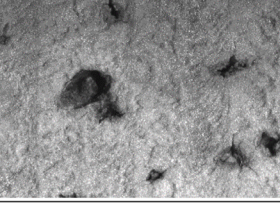

Data will be made available on request.

Acknowledgments


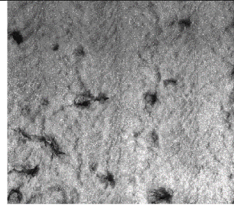


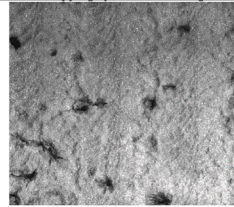

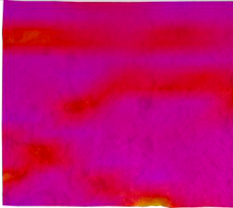
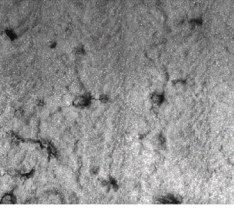

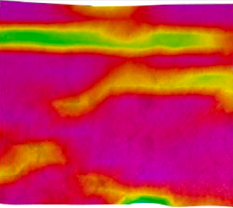
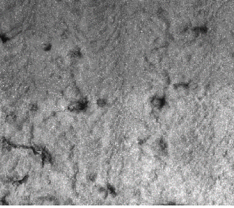

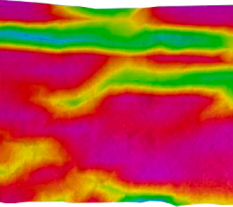
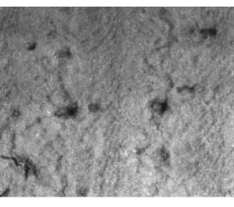

We would like to thank the regional council of Bourgogne – Franche-Comté (BFC) and the French “Investissement d’Avenir” program, project ISITE-BFC (contrat ANR-15-IDEX-003), for their financial support. We would like to thank Trescases Company for providing cork stoppers. The authors would like to thank the MIFHySTO and DIVVA facilities for the access to the equipments. The authors also thank Dr. Laurence Dujourdy for help in statistical analysis.


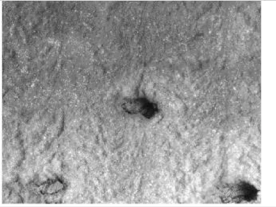


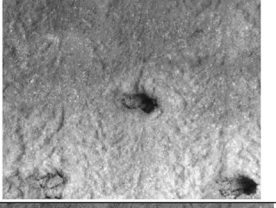
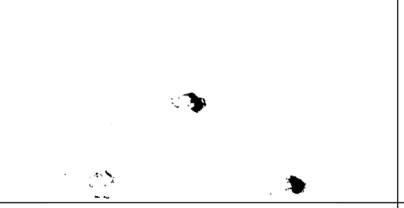
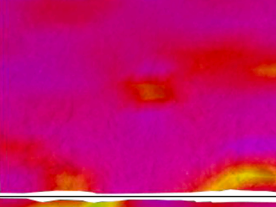
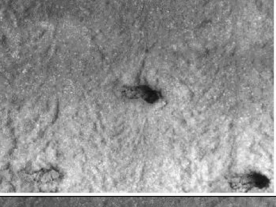
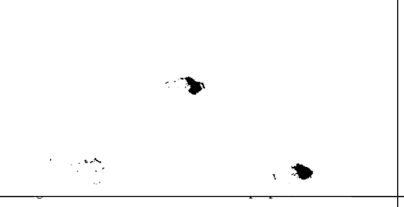
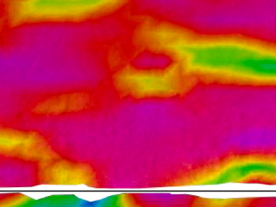

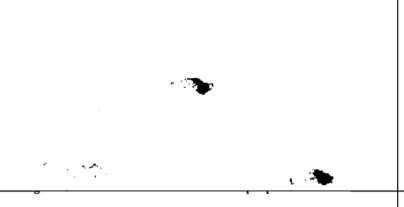
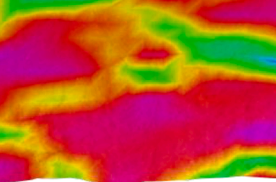
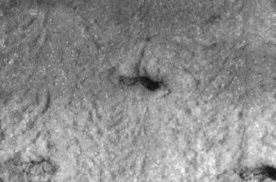

Appendix

Table 4
 DIC analysis and thresholding (after binarization) of a cork surface (cropped according to Fig. 8) performed at 0 %, 1 %, 5 %, 10 % and 15 % of nominal strain during the quasi-static compression test on a cork cube.


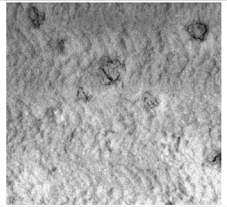


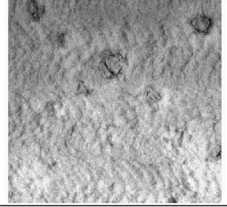

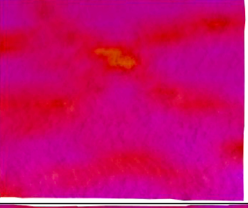
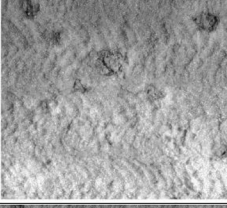
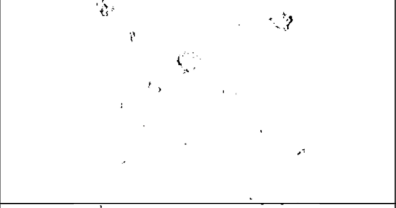
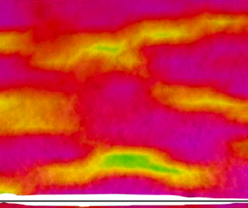
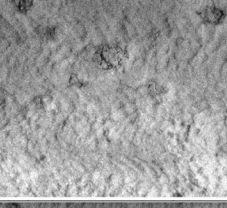
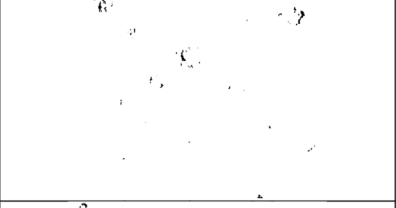
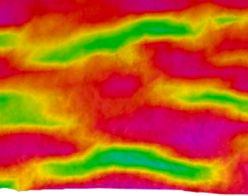
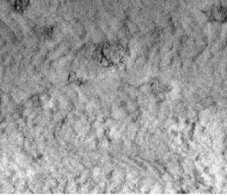

Nominal strain (%)	Strain field	DIC image	Lenticels		
			DIC image after binarization	Lenticels proportion (%)	Compression of lenticels (%)
0				3.4	0
1				3.2	4.8
5				2.6	21.8
10				2.4	27.8
15				2.2	35.8

Cube 2 (25 °C and 53 % RH).


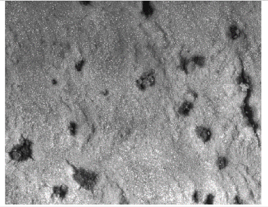


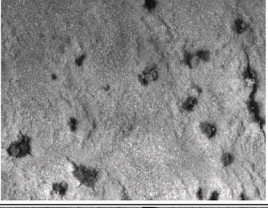
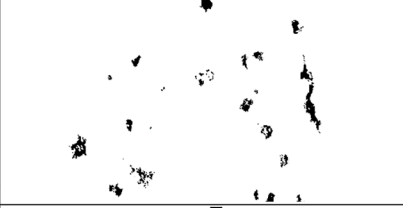
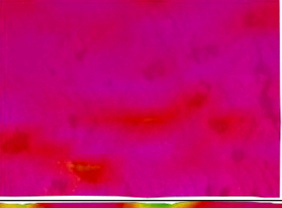
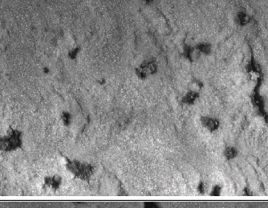

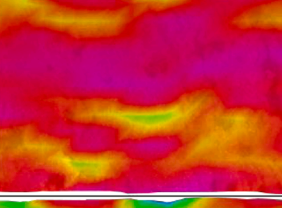
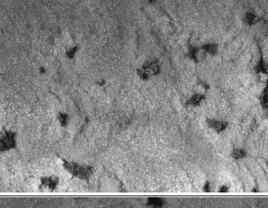
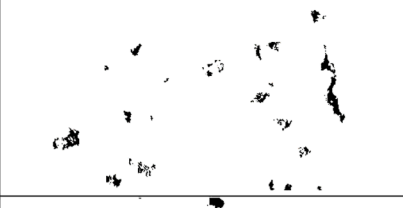
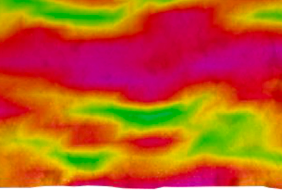
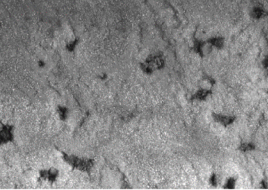

Nominal strain (%)	Strain field	DIC image	Lenticels		
			DIC image after binarization	Lenticels proportion (%)	Compression of lenticels (%)
0				1.7	0
1				1.6	8.1
5				1.3	22.7
10				1.0	42.4
15				0.9	48.8


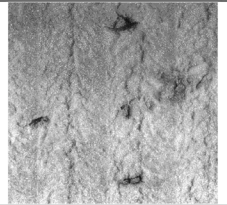


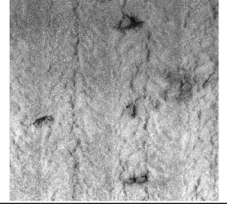

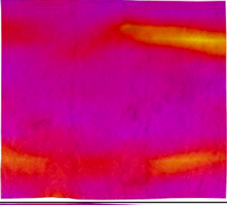
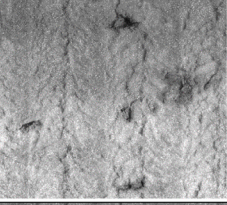

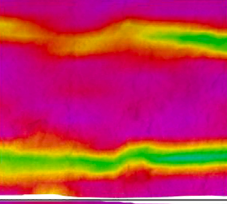
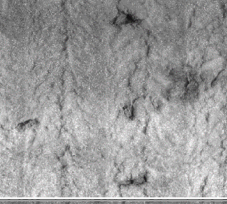
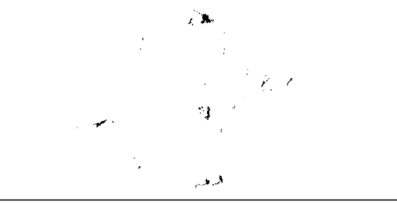
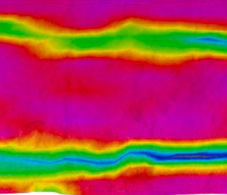
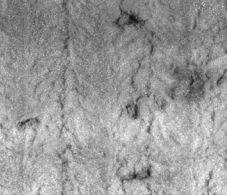

Nominal strain (%)	Strain field	DIC image	Lenticels		
			DIC image after binarization	Lenticels proportion (%)	Compression of lenticels (%)
0				0.9	0
1				0.9	5.3
5				0.7	21.3
10				0.7	25.5
15				0.6	34.0

Cube 4 (25 °C and 53 % RH).

Nominal strain (%)	Strain field	DIC image	Lenticels		
			DIC image after binarization	Lenticels proportion (%)	Compression of lenticels (%)
0				0.5	0
1				0.5	8.0
5				0.3	32.0
10				0.3	36.0
15				0.3	34.0

Cube 5 (25 °C and 53 % RH).

Nominal strain (%)	Strain field	DIC image	Lenticels		
			DIC image after binarization	Lenticels proportion (%)	Compression of lenticels (%)
0				2.8	0
1				2.7	3.9
5				2.6	8.5
10				2.4	13.5
15				2.3	17.0

Nominal strain (%)	Strain field	DIC image	Lenticels		
			DIC image after binarization	Lenticels proportion (%)	Compression of lenticels (%)
0				0.6	0
1				0.6	1.7
5				0.5	22.4
10				0.4	31.0
15				0.4	32.8

References

- [1] M. Flores, M.E. Rosa, C.Y. Barlow, M.A. Fortes, M.F. Ashby, Properties and uses of consolidated cork dust, *J. Mater. Sci.* 27 (20) (1992) 5629–5634, <https://doi.org/10.1007/BF00541634>.
- [2] J.A. Maga, J.-L. Puech, Cork and Alcoholic Beverages, *Food Rev. Intl.* 21 (1) (2005) 53–68, <https://doi.org/10.1081/FRI-200040593>.
- [3] K. Crouvisier-Urien, J.-P. Bellat, R.D. Gougeon, T. Karbowski, Gas transfer through wine closures: A critical review, *Trends Food Sci. Technol.* 78 (2018) 255–269, <https://doi.org/10.1016/j.tifs.2018.05.021>.
- [4] Gibson, L.J. and Ashby, M.F., *Cellular Solids: Structure and Properties*, 2 ed. Cambridge University Press: Cambridge, 1997.
- [5] A. Lagorce-Tachon, T. Karbowski, D. Champion, R.D. Gougeon, J.-P. Bellat, Mechanical properties of cork: Effect of hydration, *Mater. & Des.* 82 (2015) 148–154, <https://doi.org/10.1016/j.matdes.2015.05.034>.
- [6] M.E. Rosa, M.A. Fortes, Rate effects on the compression and recovery of dimensions of cork, *J. Mater. Sci.* 23 (3) (1988) 879–885, <https://doi.org/10.1007/BF01153983>.
- [7] N. Lakreb, U. Şen, E. Toussaint, S. Amziane, E. Djakab, H. Pereira, Physical properties and thermal conductivity of cork-based sandwich panels for building insulation, *Constr. Build. Mater.* 368 (2023) 130420, <https://doi.org/10.1016/j.conbuildmat.2023.130420>.
- [8] A.K. Tedjditi, F. Ghomari, O. Taleb, R. Belarbi, R. Tarik Bouhraoua, Potential of using virgin cork as aggregates in development of new lightweight concrete, *Constr. Build. Mater.* 265 (2020) 120734, <https://doi.org/10.1016/j.conbuildmat.2020.120734>.
- [9] S. Dias, A. Tadeu, J. António, J. Almeida, F. Pedro, S. Martins, C. Serra, Experimental study of expanded cork agglomerate blocks – Compressive creep behavior and dynamic performance Experimental study of expanded cork agglomerate blocks – Compressive creep behavior and dynamic performance, *Constr. Build. Mater.* 181 (2018) 551–564, <https://doi.org/10.1016/j.conbuildmat.2018.06.021>.
- [10] S. Reculosa, M. Trinquocoste, L. Dariol, P. Delhaës, Formation of low-density carbon materials through thermal degradation of a cork-based composite, *Carbon* 44 (7) (2006) 1316–1320, <https://doi.org/10.1016/j.carbon.2005.12.051>.
- [11] Pereira, H., Chapter 11 - Cork products and uses, in *Cork*, H. Pereira, Editor. 2007, Elsevier Science B.V.: Amsterdam. p. 243–261.
- [12] APCOR, *Cork Yearbook*. Associação Portuguesa da Cortiça: Av. Comendador Henrique Amorim, n.º 580, Apartado 100, 4536-904 Santa Maria de Lamas, Portugal, 2020.
- [13] Pereira, H., Chapter 2 - The structure of cork, in *Cork*, H. Pereira, Editor. 2007, Elsevier Science B.V.: Amsterdam. p. 33–53.
- [14] S.P. Silva, M.A. Sabino, E.M. Fernandes, V.M. Correlo, L.F. Boesel, R.L. Reis, Cork: properties, capabilities and applications, *Int. Mater. Rev.* 50 (6) (2005) 345–365, <https://doi.org/10.1179/174328005X41168>.
- [15] A. Lagorce-Tachon, F. Mairesse, T. Karbowski, R.D. Gougeon, J.-P. Bellat, T. Sliwa, J.-M. Simon, Contribution of image processing for analyzing the cellular structure of cork, *J. Chemom.* 32 (1) (2018), <https://doi.org/10.1002/cem.2988>.
- [16] Gibson, L.J., Easterling, K.E., and Ashby, M.F., *Proceedings of the Royal Society of London. A. Mathematical and Physical Sciences, The structure and mechanics of cork*, 1981. 377 (1769): p. 99–117. <https://doi.org/10.1098/rspa.1981.0117>.
- [17] K. Crouvisier-Urien, J. Chanut, A. Lagorce, P. Winckler, Z.i. Wang, P. Verboven, B. Nicolai, J. Lherminier, E. Ferret, R.D. Gougeon, J.-P. Bellat, T. Karbowski, Four hundred years of cork imaging: New advances in the characterization of the cork structure, *Sci. Rep.* 9 (1) (2019), <https://doi.org/10.1038/s41598-019-55193-9>.
- [18] A. Giunchi, A. Versari, G.P. Parpinello, S. Galassi, Analysis of mechanical properties of cork stoppers and synthetic closures used for wine bottling, *J. Food Eng.* 88 (4) (2008) 576–580, <https://doi.org/10.1016/j.jfoodeng.2008.03.004>.
- [19] A. Lagorce-Tachon, T. Karbowski, D. Champion, R.D. Gougeon, J.-P. Bellat, How does hydration affect the mechanical properties of wine stoppers? *J. Mater. Sci.* 51 (9) (2016) 4227–4237, <https://doi.org/10.1007/s10853-015-9669-6>.
- [20] K. Crouvisier-Urien, J.-P. Bellat, R.D. Gougeon, T. Karbowski, Mechanical properties of agglomerated cork stoppers for sparkling wines: influence of adhesive and cork particle size, *Compos. Struct.* 203 (2018) 789–796, <https://doi.org/10.1016/j.compstruct.2018.06.116>.
- [21] G. Ferreira Serra, F.A.O. Fernandes, R. J. Alves de Sousa, E. Noronha, M. Ptak, New hybrid cork-STF (Shear thickening fluid) polymeric composites to enhance head safety in micro-mobility accidents, *Compos. Struct.* 301 (2022), 116138, <https://doi.org/10.1016/j.compstruct.2022.116138>.
- [22] R.M. Coelho, R.J. Alves de Sousa, F.A.O. Fernandes, F. Teixeira-Dias, New composite liners for energy absorption purposes, *Mater. Des.* 43 (2013) 384–392, <https://doi.org/10.1016/j.matdes.2012.07.020>.
- [23] S. Gürgen, F.A.O. Fernandes, R.J.A. de Sousa, M.C. Kuşhan, Development of eco-friendly shock-absorbing cork composites enhanced by a non-newtonian fluid, *Appl. Compos. Mater.* 28 (1) (2021) 165–179, <https://doi.org/10.1007/s10443-020-09859-7>.
- [24] M. Ptak, P. Kaczyński, J. Wilhelm, J.M.T. Margarido, P.A.A.P. Marques, S.C. Pinto, R.J. Alves de Sousa, F.A.O. Fernandes, Graphene-enriched agglomerated cork material and its behaviour under quasi-static and dynamic loading, *Materials* 12 (1) (2019) 151, <https://doi.org/10.3390/ma12010151>.
- [25] Rosa, M.E. and Fortes, M.A., Temperature-induced alterations of the structure and mechanical properties of cork, *Materials Science and Engineering*, 1988. 100: p. 69–78 [https://doi.org/10.1016/0025-5416\(88\)90240-6](https://doi.org/10.1016/0025-5416(88)90240-6).
- [26] M.A. Fortes, M. Teresa Nogueira, *Materials Science and Engineering: A, The poisson effect in cork* 122 (2) (1989) 227–232, [https://doi.org/10.1016/0921-5093\(89\)90634-5](https://doi.org/10.1016/0921-5093(89)90634-5).
- [27] H. Pereira, J. Graça, C. Baptista, The effect of growth rate on the structure and compressive properties of cork, *IAWA J.* 13 (4) (1992) 389–396, <https://doi.org/10.1163/22941932-90001294>.
- [28] Oliveira, V., Rosa, M.E., and Pereira, H., *Wood Science and Technology, Variability of the compression properties of cork*, 2014. 48 (5): p. 937–948. <https://doi.org/10.1007/s00226-014-0651-2>.
- [29] Anjos, O., Pereira, H., and Rosa, M.E., *Holz als Roh- und Werkstoff, Effect of quality, porosity and density on the compression properties of cork*, 2008. 66 (4): p. 295–301. <https://doi.org/10.1007/s00107-008-0248-2>.
- [30] O. Anjos, C. Rodrigues, J. Morais, H. Pereira, Effect of density on the compression behaviour of cork, *Mater. Des.* 53 (2014) 1089–1096, <https://doi.org/10.1016/j.matdes.2013.07.038>.
- [31] L. Le Barbençon, J. Girardot, J.-B. Kopp, P. Viot, Multi-scale foam : 3D structure/compressive behaviour relationship of agglomerated cork, *Materialia* 5 (2019) 100219, <https://doi.org/10.1016/j.mtla.2019.100219>.
- [32] Sasso, M., et al., *Experimental Mechanics, Application of DIC to static and dynamic testing of agglomerated cork material*, 2018. 58 (7): p. 1017–1033. <https://doi.org/10.1007/s11340-017-0369-9>.
- [33] Sutton, M.A., Orteu, J.J., and Schreier, H., *Image correlation for shape, motion and deformation measurements: basic concepts, theory and applications*. Springer Science & Business Media 2009.
- [34] Rethoré, J. UFreckles (Version 2.0). Zenodo 2018. <https://doi.org/10.5281/zenodo.1433776>.
- [35] ISO, 9727-4: Cylindrical cork stoppers - Physical tests - Part 4 : determination of dimensional recovery after compression. 2007.
- [36] M.F. Vaz, M.A. Fortes, Friction properties of cork, *J. Mater. Sci.* 33 (8) (1998) 2087–2093, <https://doi.org/10.1023/A:1004315118535>.
- [37] J.F. Mano, The viscoelastic properties of cork, *J. Mater. Sci.* 37 (2) (2002) 257–263, <https://doi.org/10.1023/A:1013635809035>.
- [38] M.E. Rosa, M.A. Fortes, Stress relaxation and creep of cork, *J. Mater. Sci.* 23 (1) (1988) 35–42, <https://doi.org/10.1007/BF01174031>.
- [39] Rahimidehgolan, F. and Altenhof, W., *Composites Part B: Engineering, Compressive behavior and deformation mechanisms of rigid polymeric foams: A review*, 2023. p. 110–513. <https://doi.org/10.1016/j.compositesb.2023.110513>.
- [40] Y. Sun, B. Amirasouli, S.B. Razavi, Q.M. Li, T. Lowe, P.J. Withers, The variation in elastic modulus throughout the compression of foam materials, *Acta Mater.* 110 (2016) 161–174, <https://doi.org/10.1016/j.actamat.2016.03.003>.
- [41] F. Ramsteiner, N. Fell, S. Forster, *Polymer testing, Testing the deformation behaviour of polymer foams* 20 (6) (2001) 661–670, [https://doi.org/10.1016/S0142-9418\(00\)00090-8](https://doi.org/10.1016/S0142-9418(00)00090-8).